Author Manuscript

Author Manuscript

Author Manuscript

Author Manuscript

HHS Public Access

Author manuscript

Proc SPIE Int Soc Opt Eng. Author manuscript; available in PMC 2022 April 22.

Published in final edited form as:

Proc SPIE Int Soc Opt Eng. 2021 ; 11598: . doi:10.1117/12.2581708.

Lung parenchymal characterization via thoracic dynamic MRI in normal children and pediatric patients with TIS

Yubing Tong[1], **Jayaram K. Udupa**[1,*], **Joseph M. McDonough**[2], **Carina Lott**[2], **Caiyun Wu**[1], **Chamith S. Rajapakse**[3], **Jason B. Anari**[2], **Drew A. Torigian**[1], **Patrick J. Cahill**[2]

[1]Medical Image Processing Group, Department of Radiology, University of Pennsylvania, Philadelphia, PA, 19104, United States

[2]The Wyss/Campbell Center for Thoracic Insufficiency Syndrome, Children's Hospital of Philadelphia, Philadelphia, PA, 19104, United States

[3]Department of Radiology and Department of Orthopedic Surgery, University of Pennsylvania, Philadelphia, PA, 19104, United States

Abstract

Quantitative thoracic dynamic magnetic resonance imaging (QdMRI), a recently developed technique, provides a potential solution for evaluating treatment effects in thoracic insufficiency syndrome (TIS). In this paper, we demonstrate how lung parenchymal characteristics can be assessed via intensity properties in lung dynamic MRI, a modality suitable for use in pediatric patients. The QdMRI-based approach includes dynamic MR image acquisition, 4D image construction, image pre-processing with non-uniformity correction and intensity standardization, and lung segmentation from the 4D constructed image via a deep learning approach, as well as extraction of image parenchymal intensity properties from the segmented lungs and statistical comparisons among different clinical scenarios. We include 22 dMRI scans from 11 TIS patients (each with both pre-operative and post-operative scans) and 23 dMRI scans from healthy children. Two-sided paired t-testing is performed to compare lung intensity properties between end of expiration (EE) and end of inspiration (EI) within TIS patients (pre-operative and post-operative, separately) and normal children. We also compare the lung intensity properties at EE and EI among pre-operative TIS patients, post-operative TIS patients, and normal children. Experimental results show that lung (T2) intensity at EI is significantly lower than that at EE and lung intensity of post-operative TIS patients is significantly lower than that in pre-operative TIS patients and closer to that of normal children than to that of pre-operative TIS patients, indicating improvement in lung aeration. To our knowledge, this is the first study to provide a quantitative dynamic functional method to analyze lung parenchyma during tidal breathing on dynamic MRI in both healthy children and pediatric patients with TIS.

Keywords

lung parenchyma; 4D construction; dynamic MRI; thoracic insufficiency syndrome (TIS); lung aeration

*Corresponding author.

Author Manuscript Author Manuscript Author Manuscript Author Manuscript

1. INTRODUCTION

Thoracic insufficiency syndrome (TIS) is a rare but serious disorder that involves thoracic respiratory abnormality associated with over 27 pediatric syndromes [1]. One challenge in the management of patients with TIS treatment is that current treatment is predominantly dependent upon the experience of surgeons given that there are only a few quantitative measures available for treatment planning and evaluation of treatment effects. Quantitative thoracic dynamic MRI (QdMRI), a recently developed technique [2], provides a potential solution to this hurdle. We have utilized the QdMRI technique to depict changes in dynamic function of the lungs and chest for both TIS patients (before and after surgical correction [3]) and normal children ([4]) by assessing volumes at the end of inspiration (EI) and end of expiration (EE) for each lung, each hemi-diaphragm, and each chest wall during one free-breathing cycle. QdMRI enables chest wall motion analysis in early onset scoliosis by comparing the chest wall excursion volume before and after surgery, as well as the analysis of the association between pulmonary hypertension and thoracic cage function [3]. We have also illustrated on data sets of healthy children that QdMRI could quantify changes in the components of ventilatory pump dynamics during childhood [4]. However, changes in lung tissue characteristics have not yet been studied in the past due to the lack of simple and readily usable non-invasive techniques. Such studies can be especially useful in better understanding lung physiology during normal growth and in TIS patients before and after corrective procedures.

In this paper, we investigate the use of QdMRI to characterize lung parenchyma to fill this gap for studying lung ventilation. Computed tomography (CT) [5], hyperpolarized ^{129}Xe MRI [6], hyperpolarized ^{3}He MRI [7], and single plane 2D dynamic MRI [8] have previously been used in lung parenchymal analysis of ventilation and perfusion. However, CT is associated with radiation exposure [5] and the other techniques are predominantly used for research purposes given difficulties in clinical implementation [6,7] or requirement for breath-holding during image acquisition [8, 9]. For many TIS patients, other patient populations, and young normal children, it is difficult to cooperate with breathing instructions during image acquisition. QdMRI is a purely image-based approach and is designed to utilize images acquired under free tidal breathing conditions, which makes it practical for implementation in clinical practice. To our knowledge, this is the first study to provide a quantitative dynamic functional method for lung parenchymal characterization, not only on TIS patients (pre-operative and post-operative), but also on normal children.

2. MATERIALS & METHODS

Image data

All data were acquired under an ongoing research protocol approved by the Institutional Review Board at the Children's Hospital of Philadelphia (CHOP) and University of Pennsylvania, along with Health Insurance Portability and Accountability Act waiver. We included 22 dynamic thoracic MRI scans from 11 TIS patients, each with both pre-operative and post-operative (after VEPTR surgery [1]) scans. We also enrolled 23 healthy children

Author Manuscript Author Manuscript Author Manuscript Author Manuscript

ages 6 to 14 years with the exclusion criteria: (i) history of thoracic surgery; (ii) history of asthma or other lung disease; (iii) respiratory tract illness within the last 30 days; and (iv) history of scoliosis or other congenital skeletal abnormality. Table 1 summarizes data sets from TIS patients and normal children employed in this study.

Methods

QdMRI-based lung parenchymal analysis includes the following steps: (i) free-breathing dynamic MR image acquisition, (ii) 4D image construction, (iii) image processing for intensity non-uniformity correction and intensity standardization, (iv) lung segmentation in 4D constructed image, and (v) extraction of image intensity properties within segmented lung regions and statistical comparisons among different clinical scenarios to seek signatures related to tissue aeration.

(i) dMRI data acquisition: The thoracic dMRI protocol was performed as follows: 3T MRI scanner (Verio, Siemens, Erlangen, Germany), True-FISP sequence, TR=3.82 ms, TE=1.91 ms, voxel size ~1×1×6 mm^3, 320×320 matrix, bandwidth 258 Hz, and flip angle 76°. For each sagittal location across the thorax, 80 slices were obtained over several tidal breathing cycles at ~480 ms/slice. On average, 35 sagittal locations across the chest were imaged. Therefore, a total of 2800 (35 × 80) 2D MRI slices were available to construct one representative 4D image comprising one full breathing cycle of the subject.

(ii) 4D image construction: We utilized our recently developed optical-flux-based 4D image construction approach [2], which is a purely image-based and fully automated algorithm. Compared to previous 4D construction methods, the new approach can handle deep and shallow breaths as well as body shifting among neighboring locations, and has no requirement for obtaining surrogate breathing signals, making image construction more efficient. The new approach achieves remarkable spatial and temporal continuity for all subjects. Over all tested data sets and cycles, temporal disorderliness is less than 0.1, and the objective non-smoothness factor is less than 1-pixel unit for all subjects. More details can be found in [2].

(iii) Image processing: Image intensity non-uniformity correction and intensity standardization were applied to the 4D constructed images. Intensity standardization allows MR intensity values to attain tissue-specific numeric meaning. Previous research has shown that these operations are vital for quantitative analysis of MR images [10]. In this study, calibration parameters for intensity standardization were estimated based on a normal children data set and were utilized to standardize both normal-subject and patient data sets. More details of intensity standardization can be found in [10].

(iv) Lung segmentation: A 2D U-Net [11] type of deep learning (DL) network was implemented to segment lung in the constructed and intensity corrected/standardized 4D image. Since segmentation is not the major issue addressed in this paper, we briefly describe the DL-based lung segmentation strategy. A properly designed DL network can facilitate lung segmentation in pediatric chest dynamic MRI, which is particularly challenging due to low image quality and motion blur [12– 15]. The basic idea is to train a model using normal

Author Manuscript Author Manuscript Author Manuscript Author Manuscript

children data and then use the trained model to segment lungs in TIS patient and normal children data sets. We utilized 23 4D MRI data sets from normal children for training and subsequent testing of the segmentation method. First, we manually segmented each of the 3D lungs at their respective EE and EI time points in the breathing cycle. That yielded 46 segmented 3D images. We utilized 40 of these 3D image data sets (comprised of ~1,400 slices) for training the DL network and the remaining six 3D image data sets for testing. This process was repeated for 8 different combinations of training/testing data set division. The mean and standard deviation of the Dice coefficient over test data sets was found to be 0.95 ± 0.01. We also visually compared automatic segmentation results with their manually segmented counterparts and found that all results were visually acceptable. Subsequently, we utilized the trained DL network to segment each lung in 22 TIS 4D MR images. All segmentation results from TIS patients were also visually checked and manually refined if necessary, under supervision of an experienced radiologist with expertise in chest MRI. We set up the U-Net network with 200 epochs, 300 steps/epoch, and batch size 8 using one NVIDIA GeForce @Rtx2080 GPU with 8 Gbyte RAM on a computer with 64-bit Ubuntu 18.04 OS.

(v) Statistical analysis: We estimated standardized image intensity properties within segmented lung regions. This included mean, median, mode, maximum, and minimum values of the standardized intensity. Two-sided paired t-testing was used to compare the intensity properties between EE and EI conditions for TIS patients separately both pre-operatively and post-operatively. A similar analysis comparing EE and EI conditions was also carried out on normal children data sets. We also compared the lung intensity properties at EE and EI between (pre-operative/post-operative) TIS patients and normal children by using two-sided unpaired t-testing.

3. RESULTS

Figure 1 (top row) shows lung segmentations at EE and EI for one TIS patient (female, pre-operative – 3 yrs, post-operative – 7 yrs), and one normal child (male, 9 yrs). We set up the same display window for the TIS patient and the normal child. 3D surface renditions are shown in the 2nd row by overlaying surfaces from EE (in gray) and EI (in color). Observe that the volume of the lungs at EI is larger than that at EE and that the signal intensity of the lungs at EI in all instances is lower (appears darker) than that at EE for each case. The image intensity of the lung at EI for the post-operative TIS patient was much closer to that of the normal child compared to image intensity at EI of the pre-operative TIS patient to that of normal child.

Table 2 summarizes quantitative lung intensity properties at EE and EI for TIS patients, pre-operative, and post-operative separately, as well as for normal children. P values from paired t-testing of the intensity properties between EE and EI are also listed. Note that the statistics listed (mean, median, etc.) are for the whole group of subjects under each category and are not relevant for paired t-tests. In the paired t-test, we observed a very strong within-subject correlation of 0.967. This strong and consistent lowering of subject-wise intensity from EE to EI in the paired t-test suggests increased tissue aeration from EE to EI within each of the three situations – pre-op, post-op, and normal.

Author Manuscript Author Manuscript Author Manuscript Author Manuscript

Table 3 shows the p values from comparisons of standardized signal intensities among TIS pre-operative patients, TIS post-operative patients, and normal children. Note that patient-to-normal-subject comparison is (has to be) group-wise and not paired. In the paired comparison at EI, with the patient as his/her own reference, image intensity becomes lower post-operatively with statistical significance ($p = 0.003$) suggesting improved lung tissue aeration post-operatively. A similar observation can be made about signal intensity change at EE but only with marginal statistical significance ($p = 0.06$). Interestingly, in comparing tissue intensity group-wise at both EE and EI with corresponding tissue intensity of normal children, group-wise mean intensities (see Table 2) in TIS patients are higher than group-wise mean intensity for normal subjects in corresponding conditions. Post-operatively, however, group-wise mean intensity at EI is closer to group-wise mean intensity at EI for normal subjects than the group-wise mean intensities at EE.

We are in the process of collecting more data sets and also performing a phantom experiment to provide further evidence that our QdMRI system actually measures the change in air content with a level of sensitivity that is sufficient for the TIS application.

4. CONCLUSIONS

We present a novel and practical approach for lung parenchymal characterization via thoracic dynamic MRI for both TIS patients (for studying physiological changes due to treatment) and normal children (for studying change in physiology due to maturation). Experimental results show that lung intensity at EI is significantly lower than that at EE, and that lung intensity of post-operative TIS patients is significantly lower than that in the pre-operative state, indicating post-surgical improvements in lung aeration. The lung intensity of post-operative TIS patients is closer to that of normal children than the lung intensity in pre-operative TIS patients compared to that in normal children. This study provides a practical approach for studying physiological changes in lung parenchyma in pediatric TIS and in other pediatric and adult applications using dynamic MRI.

Acknowledgment

This research is supported by a grant 1R01HL150147-01 from the National Institutes of Health. This research is also supported by in part by the Institute for Translational Medicine and Therapeutics of the University of Pennsylvania through a grant by the National Center for Advancing Translational Sciences of the National Institutes of Health under award number UL1TR001878.

References

[1]. Campbell RM Jr., Smith MD. Thoracic insufficiency syndrome and exotic scoliosis. J Bone Joint Surg Am. 2007;89 Suppl 1:108–22. [PubMed: 17272428]

[2]. Hao Y, Udupa JK, Torigian DA. 4D image construction from free-breathing MRI slice acquisitions of the thorax based on a concept of flux. Proc SPIE Int Soc Opt Eng. 2020;11312.

[3]. Tong Y, Udupa JK, McDonough JM, Mayer OH, Torigian DA, Campbell RM. Quantitative Dynamic Thoracic MRI: Application to Thoracic Insufficiency Syndrome in Pediatric Patients. Radiology. 2019;292(1):206–13. [PubMed: 31112090]

[4]. Tong Y, Udupa JK, McDonough JM, Wu C, Sun C, Qiu C, Lott C, Galagedera N, Anari JB, Mayer OH, Torigian DA, Cahill PJ. Thoracic quantitative dynamic MRI to understand developmental changes in normal ventilatory dynamics. Chest. 2020. doi: 10.1016/j.chest.2020.07.066.

Author Manuscript Author Manuscript Author Manuscript Author Manuscript

[5]. Washko GR, Parraga G, Coxson HO. Quantitative pulmonary imaging using computed tomography and magnetic resonance imaging. Respirology. 2012;17(3):432–444. [PubMed: 22142490]

[6]. Mugler JP 3rd, Altes TA. Hyperpolarized ^{129}Xe MRI of the human lung. J Magn Reson Imaging. 2013;37(2):313–331. [PubMed: 23355432]

[7]. Fain S, Schiebler ML, McCormack DG, Parraga G. Imaging of lung function using hyperpolarized helium-3 magnetic resonance imaging: Review of current and emerging translational methods and applications. J Magn Reson Imaging. 2010;32(6):1398–1408. [PubMed: 21105144]

[8]. Levin DL, Chen Q, Hatabu H. Evaluation of regional pulmonary perfusion using ultrafast magnetic resonance imaging. Magn Reson Med. 2001; 46:166–171. [PubMed: 11443723]

[9]. Biederer J, Beer M, Hirsch W et al. MRI of the lung (2/3). Why … when … how?. Insights Imaging. 2012; 3, 355–371. [PubMed: 22695944]

[10]. Zhuge Y, Udupa JK, Liu J, Saha PK. Image background inhomogeneity correction in MRI via intensity standardization, Comput Med Imaging Graph., 2009; 33(1):7–16. [PubMed: 19004616]

[11]. Ronneberger O, Fisher P, Brox T. U-Net: Convolutional Networks for Biomedical Image Segmentation. CVPR 2015, https://arxiv.org/pdf/1505.04597.pdf.

[12]. Choi KS, You SH, Han Y, Ye JC, Jeong B, Choi SH. Improving the Reliability of Pharmacokinetic Parameters at Dynamic Contrast-enhanced MRI in Astrocytomas: A Deep Learning Approach. Radiology. 2020;297(1):178–88. [PubMed: 32749203]

[13]. Biswas S, Aggarwal HK, Jacob M. Dynamic MRI using model-based deep learning and SToRM priors: MoDL-SToRM. Magn Reson Med. 2019;82(1):485–94. [PubMed: 30860286]

[14]. Jiang J, Hu YC, Tyagi N, Zhang P, Rimner A, Deasy JO, Veeraraghavan H. Cross-modality (CT-MRI) prior augmented deep learning for robust lung tumor segmentation from small MR datasets. Med Phys. 2019;46(10):4392–404. [PubMed: 31274206]

[15]. Duan C, Deng H, Xiao S, Xie J, Li H, Sun X, Ma L, Lou X, Ye C, Zhou X. Fast and accurate reconstruction of human lung gas MRI with deep learning. Magn Reson Med. 2019;82(6):2273–85. [PubMed: 31322298]

Author Manuscript Author Manuscript Author Manuscript Author Manuscript

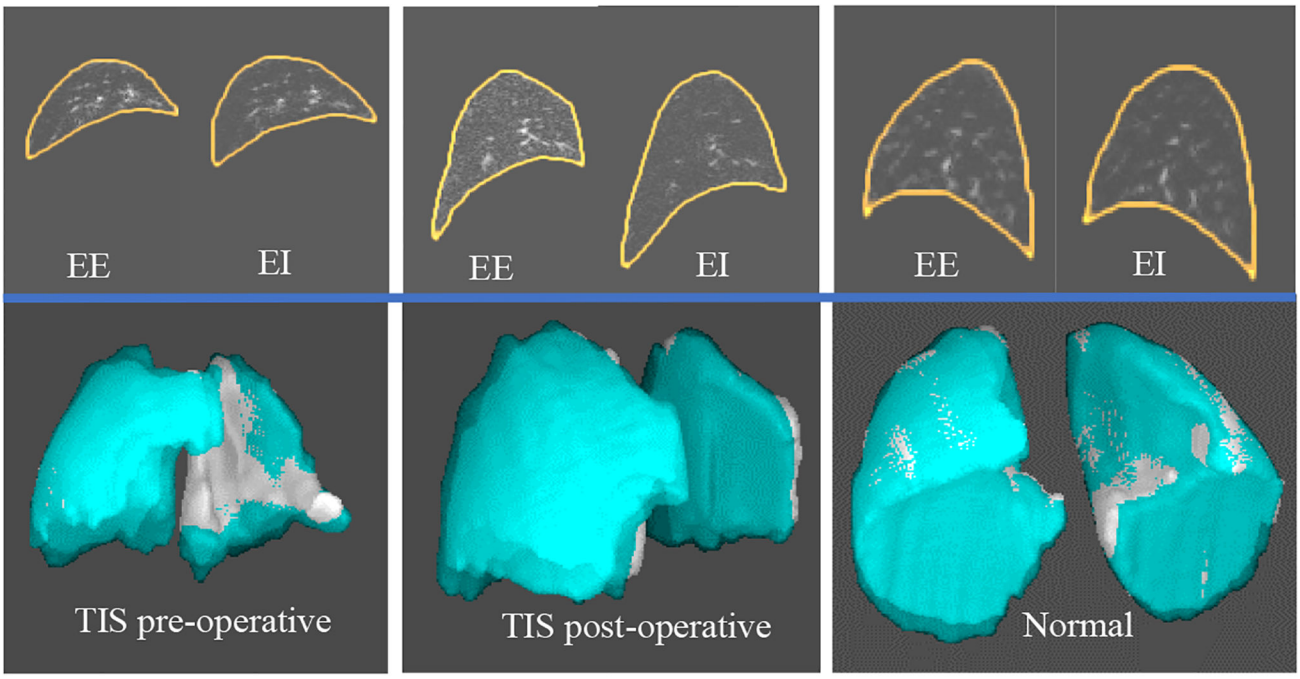

Figure 1.
An example of segmented lung with image intensity (top row) and 3D surface renditions (bottom row) for one TIS patient (pre-operative and post-operative) and one normal child.

Author Manuscript

Author Manuscript

Author Manuscript

Author Manuscript

Table 1.

Data sets for lung parenchyma analysis via QdMRI.

	Condition	Subjects	Age (years)	Number of respiratory phases in one 4D image	3D images analyzed
TIS	Pre-op	6M, 5F	4.99 ± 4.14	6.09 ± 1.86	67
	Post-op		6.83 ± 3.89	6.64 ± 2.34	73
Normal		11M, 12F	9.51 ± 1.57	5.78 ± 1.78	133

Author Manuscript

Author Manuscript

Author Manuscript

Author Manuscript

Table 2.

Intensity properties of lung parenchyma from dynamic MRI at end of expiration (EE) and end of inspiration (EI) for TIS patients (pre-operative (Pre-op) and post-operative (Post-op)) and normal children. Mean ± standard deviation and p values from paired t-testing between EE and EI are shown. P values less than 0.05 are highlighted in bold.

		Mean	Median	Mode	Maximum	Minimum
TIS Pre-op	EI	112 ± 52	64 ± 31	36 ± 16	3759 ± 460	0 ± 0
	EE	136 ± 64	81 ± 44	41 ± 25	3723 ± 452	0 ± 0
	p: EE vs. EI	**0.001**	**0.007**	0.30	0.70	N/A
TIS Post-op	EI	82 ± 39	49 ± 24	31 ± 16	3719 ± 637	0 ± 0
	EE	112 ± 39	66 ± 23	37 ± 12	3661 ± 634	0 ± 0
	p: EE vs. EI	**0.003**	**0.006**	0.06	0.69	N/A
Normal	EI	54 ± 12	24 ± 5	10 ± 2	1990 ± 631	0 ± 0
	EE	58 ± 12	26 ± 5	11 ± 2	2074 ± 770	0 ± 0
	p: EE vs. EI	< **0.001**	< **0.001**	0.21	0.40	N/A

Author Manuscript

Author Manuscript

Author Manuscript

Author Manuscript

Table 3.

Lung parenchymal intensity property comparison between pre-operative TIS patients, post-operative TIS patients, and normal children. P values less than 0.05 are highlighted in bold.

	Mean	Median	Mode	Maximum	Minimum
TIS Pre-op vs. Post-op at EI, paired t-test	**0.003**	**0.003**	**0.008**	0.88	N/A
TIS Pre-op vs. Post-op at EE, paired t-test	0.06	0.13	0.54	0.82	N/A
TIS Pre-op vs. normal at EI, unpaired t-test	**0.004**	**0.002**	**< 0.001**	**< 0.001**	N/A
TIS Pre-op vs. normal at EE, unpaired t-test	**0.002**	**0.002**	**0.002**	**< 0.001**	N/A
TIS Post-op vs. normal at EI, unpaired t-test	**0.04**	**0.007**	**0.002**	**< 0.001**	N/A
TIS Post-op vs. normal at EE, unpaired t-test	**0.001**	**< 0.001**	**< 0.001**	**< 0.001**	N/A